Earth Planets Space, **60**, 763–771, 2008

Effects of latitudinal distributions of particle density and wave power on cyclotron resonant diffusion rates of radiation belt electrons

Danny Summers and Binbin Ni

Department of Mathematics and Statistics, Memorial University of Newfoundland, St. John's, Newfoundland, Canada

(Received February 8, 2008; Revised March 25, 2008; Accepted March 26, 2008; Online published August 4, 2008)

We evaluate cyclotron resonant interactions of radiation belt electrons with VLF chorus, plasmaspheric ELF hiss and electromagnetic ion cyclotron (EMIC) waves. We assume that the Earth's magnetic field is dipolar and that each wave mode has a Gaussian spectral density. The dependence of the resonant electron diffusion rates on the latitudinal distributions of particle density and wave power is examined. We find that while the diffusion rates can be sensitive to the latitudinal distributions of density and wave power, in general the sensitivity depends on wave mode, equatorial pitch-angle, electron energy and L-shell. We determine the effects of the latitudinal distributions of density and wave power on the electron precipitation loss timescale due to combined scattering by VLF chorus, ELF hiss and EMIC waves. Accurate modeling of radiation belt electron dynamics requires observational data on the global distributions of particle number density and wave power.

Key words: Earth's radiation belt, wave-particle interactions, magnetospheric plasma waves, electron precipitation.

1. Introduction

Electrons in the Earth's outer radiation belt ($3 < L < 7$) undergo cyclotron resonant interactions with various modes of plasma wave including whistler-mode chorus, plasmaspheric hiss and electromagnetic ion cyclotron (EMIC) waves, e.g., see Summers *et al*. (2007a, b) and references therein. Whistler-mode (VLF) chorus waves are observed in the lower-density region outside the plasmasphere, typically in the frequency range 0.05–0.8Ω_e, where Ω_e is the electron gyrofrequency (Meredith *et al*., 2001; Santolik *et al*., 2004). Hiss is a broadband whistler-mode ELF emission occurring inside the plasmasphere and drainage plumes in the frequency range ∼100 Hz–several kHz (Meredith *et al*., 2004). EMIC waves in the frequency range 0.1–5.0 Hz are observed in the plasmasphere, typically along the duskside plasmapause, and in drainage plumes (Fraser and Nguyen, 2001). Energy diffusion due to cyclotron resonance with VLF chorus is an effective mechanism for generating relativistic (>1 MeV) electrons in the outer radiation belt during magnetic storms (Summers *et al*., 1998, 2002; Roth *et al*., 1999; Summers and Ma, 2000; Miyoshi *et al*., 2003; Horne *et al*., 2005; Omura and Summers, 2006). VLF chorus, ELF hiss, and EMIC waves can each cause pitch-angle scattering of electrons into the loss cone leading to precipitation losses from the outer zone (Summers and Thorne, 2003; Albert, 2003; Thorne *et al*., 2005).

Quasi-linear theory provides useful techniques for determining the average properties of cyclotron-resonant diffusion (e.g., Lyons, 1974; Summers, 2005; Albert, 2007). Summers *et al*. (2007a, b) calculate quasi-linear diffusion rates to determine timescales for radiation belt electron acceleration and loss due to cyclotron resonance with VLF chorus, ELF hiss and EMIC waves. Resonant diffusion rates depend on the assumed distributions of background particle density and wave power. The present investigation extends the work of Summers *et al*. (2007a, b) by examining the effects of latitudinal distributions of particle density and wave power on the resonant diffusion rates of radiation belt electrons for the aforementioned wave modes. In Section 2 we provide a short account of the quasi-linear theory required to calculate resonant diffusion rates. In Section 3 we present our calculations of the (bounce-averaged) electron diffusion rates for individual wave modes, and we also determine the effects of the latitudinal distributions of density and wave power on electron precipitation loss timescales due to combined scattering by VLF chorus, ELF hiss and EMIC waves. Finally, in Section 4 we summarize our results.

2. Cyclotron Resonant Diffusion Rates

We assume a homogeneous collisionless plasma immersed in a uniform background magnetic field in the presence of superposed electromagnetic waves. The relativistic quasi-linear diffusion equation for the gyrophase-averaged phase space density Φ is

$$\frac{\partial \Phi}{\partial t} = \frac{1}{\sin\alpha}\frac{\partial}{\partial\alpha}\left(D_{\alpha\alpha}\ \sin\alpha\ \frac{\partial\Phi}{\partial\alpha}\right) + \frac{1}{\sin\alpha}\frac{\partial}{\partial\alpha}\left(D_{\alpha p}\ \sin\alpha\ \frac{\partial\Phi}{\partial p}\right) + \frac{1}{p^2}\frac{\partial}{\partial p}\left(p^2\ D_{p\alpha}\ \frac{\partial\Phi}{\partial\alpha}\right) + \frac{1}{p^2}\frac{\partial}{\partial p}\left(p^2\ D_{pp}\ \frac{\partial\Phi}{\partial p}\right), \quad (1)$$

Copyright © The Society of Geomagnetism and Earth, Planetary and Space Sciences (SGEPSS); The Seismological Society of Japan; The Volcanological Society of Japan; The Geodetic Society of Japan; The Japanese Society for Planetary Sciences; TERRAPUB.

where $D_{\alpha\alpha}$, $D_{\alpha p} = D_{p\alpha}$, and D_{pp} are the cyclotron resonant diffusion coefficients which depend on the properties of the waves; $p = \gamma m v$ is the particle momentum where v is the particle speed and m is the rest mass; $\gamma = \left(1 - v^2/c^2\right)^{-1/2}$ is the Lorentz factor (c is the speed of light); α is the pitch-angle, and t denotes time. The diffusion coefficients,

$$\begin{aligned} D_{\alpha\alpha} &= \overline{(\Delta\alpha)^2}/(2\Delta t), \\ D_{\alpha p} &= \overline{(\Delta\alpha)(\Delta p)}/(2\Delta t), \\ D_{pp} &= \overline{(\Delta p)^2}/(2\Delta t) \end{aligned} \tag{2}$$

are determined from the ensemble-averaged particle-orbit corrections. Explicit formulae for $D_{\alpha\alpha}$, $D_{\alpha p}$, D_{pp} corresponding to field-aligned (R-mode and L-mode) electromagnetic waves have been derived by Summers (2005) and Summers *et al.* (2007a). We assume that the waves have a Gaussian spectral density of the form,

$$\tilde{W}(\omega) = \frac{(\Delta B)^2}{8\pi} \frac{1}{\rho} \frac{1}{\delta\omega} e^{-\left(\frac{\omega-\omega_m}{\delta\omega}\right)^2}, \tag{3}$$

with

$$\rho = \frac{\sqrt{\pi}}{2} \left[\mathrm{erf}\left(\frac{\omega_m - \omega_1}{\delta\omega}\right) + \mathrm{erf}\left(\frac{\omega_2 - \omega_m}{\delta\omega}\right) \right], \tag{4}$$

where ω is the wave frequency, ω_1 is the lower frequency limit, ω_2 is the upper frequency limit, ω_m is the frequency of maximum wave power, $\delta\omega$ is a measure of the bandwidth, and erf is the error function. The wave spectral density (3) has been normalized so that

$$\frac{(\Delta B)^2}{8\pi} = \int_{\omega_1}^{\omega_2} \tilde{W}(\omega)\, d\omega \tag{5}$$

where ΔB is the mean wave amplitude.

In the present study we consider electron interaction with (R-mode) VLF chorus, (R-mode) ELF hiss, and (L-mode) EMIC waves. We assume a hydrogen plasma and we consider only field-aligned waves. Under the conditions of field-aligned wave propagation, all cyclotron harmonics n are omitted except $n = -1$ and $n = +1$ which correspond respectively to R-mode and L-mode waves. In many cases first-order-harmonic diffusion rates provide a good approximation to diffusion rates for oblique waves calculated using higher-order resonances. For a given wave mode, the local diffusion coefficients can be expressed as functions of particle kinetic energy, $E = E_k/\left(m c^2\right) = \gamma - 1$, and pitch-angle α. The diffusion coefficients depend further on the electron gyrofrequency Ω_e, the cold-plasma parameter $\alpha^* = \Omega_e^2/\omega_{pe}^2$ where ω_{pe} is the electron plasma frequency, and the wave parameters ω_1, ω_2, ω_m, $\delta\omega$, and ΔB (Summers, 2005; Summers *et al.*, 2007a). In order to calculate diffusion rates in a magnetic mirror geometry such as the Earth's magnetic field, the local diffusion coefficients $D_{\alpha\alpha}$, $D_{\alpha p}$, D_{pp} must be bounce-averaged, i.e., averaged over particle bounce orbits. Summers *et al.* (2007a) have carried out this procedure assuming a dipole magnetic field to obtain the bounce-averaged diffusion coefficients $\langle D_{\alpha\alpha}\rangle$, $\langle D_{\alpha p}\rangle$, $\langle D_{pp}\rangle$ as functions of the kinetic energy E and the equatorial pitch-angle α_{eq} of the particle. In the following section we utilize the bounce-averaged diffusion coefficients given by Summers *et al.* (2007a) to determine how diffusion rates for radiation belt electrons depend on the latitudinal distributions of particle density and wave power.

3. Results

3.1 Electron interaction with whistler-mode chorus

Whistler-mode chorus comprises short ($\sim 10^{-1}$ sec) discrete emissions that are quasi-monochromatic (e.g., Santolik *et al.*, 2004). Electron interaction with such narrowband phase-coherent emissions cannot strictly be treated by quasi-linear theory. Nevertheless, herein we average over a specified band of chorus, and we assume that chorus can be represented by a weakly turbulent continuous spectrum. Accordingly, quasi-linear theory can be expected to provide an overall description of cyclotron resonant diffusion, though a quasi-linear treatment cannot take account of nonlinear effects such as phase trapping by the wave field.

In Fig. 1 we plot the bounce-averaged pitch-angle diffusion rate $\langle D_{\alpha\alpha}\rangle$, mixed (pitch-angle/momentum) diffusion rate $\langle |D_{\alpha p}| \rangle / p$ and momentum diffusion rate $\langle D_{pp} \rangle / p^2$ for whistler-mode chorus for electron energies 100, 200, 500, 1000 keV at $L = 4$. We adopt a Gaussian wave spectral density with $\omega_1 = 0.05\Omega_e$, $\omega_2 = 0.65\Omega_e$, $\omega_m = 0.35\Omega_e$, $\delta\omega = 0.15\Omega_e$, $\Delta B = 100$ pT, and we assume that the wave amplitude is constant along the field line. We compare the case of particle density $N(\lambda) = \text{constant} = N_{eq}$ with that in which N varies as the dipole magnetic field strength, namely, $N(\lambda)/N_{eq} = B(\lambda)/B_{eq} = f(\lambda) =$

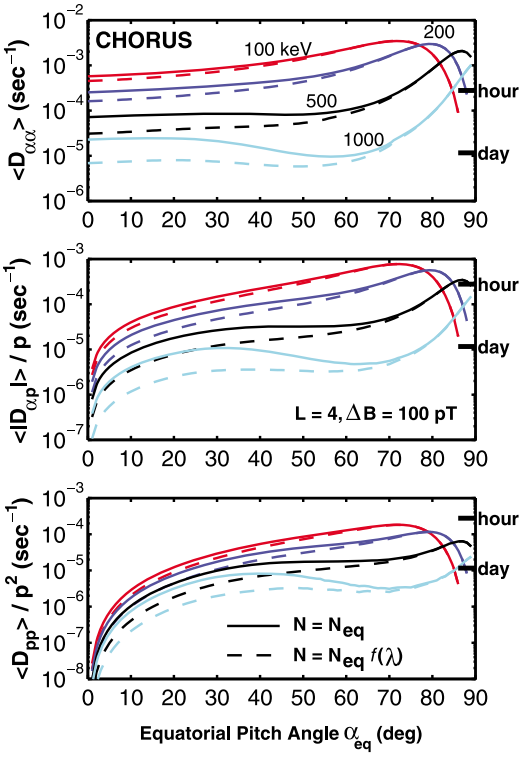

Fig. 1. Bounce-averaged diffusion coefficients for whistler-mode chorus for the indicated electron energies at $L = 4$. Two latitudinal distributions of particle density are specified: (a) $N(\lambda) = N_{eq}$= constant, (b) $N(\lambda) = N_{eq} f(\lambda)$ where $f(\lambda) = (1 + 3\sin^2\lambda)^{1/2}/\cos^6\lambda$.

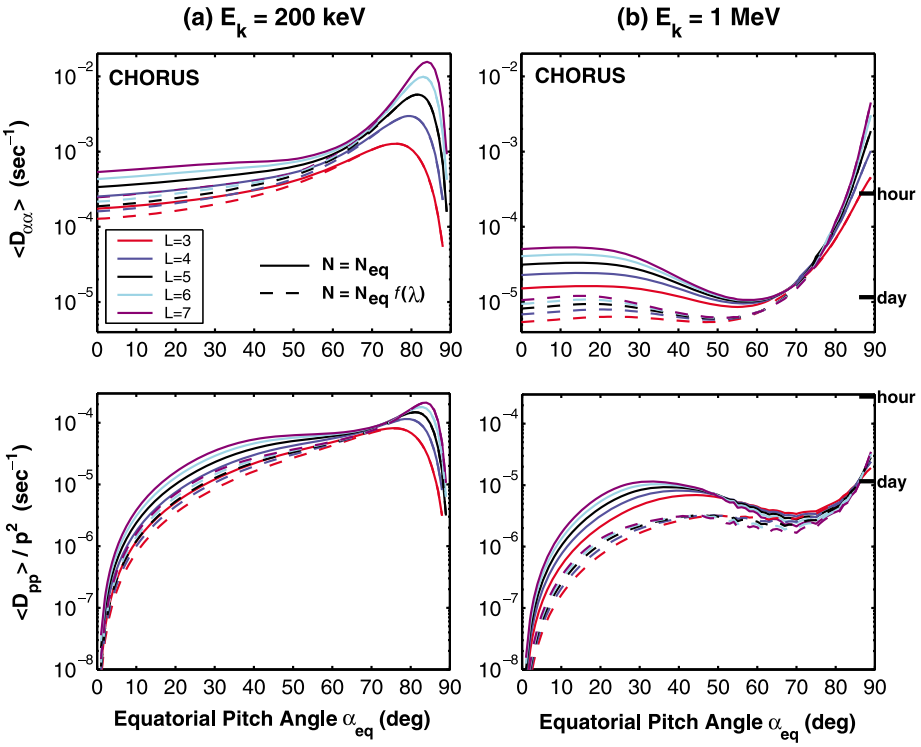

Fig. 2. Bounce-averaged pitch-angle diffusion rates (top) and momentum diffusion rates (bottom) for whistler-mode chorus for the indicated electron energies and L-values. The two chosen latitudinal distributions of particle density are as specified in Fig. 1.

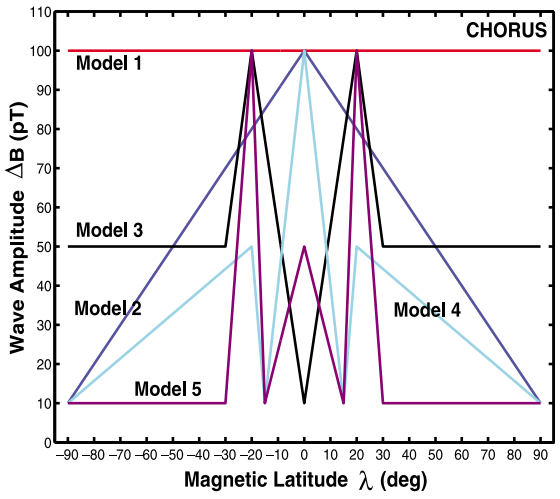

Fig. 3. Five models for the latitudinal distribution of chorus wave amplitude.

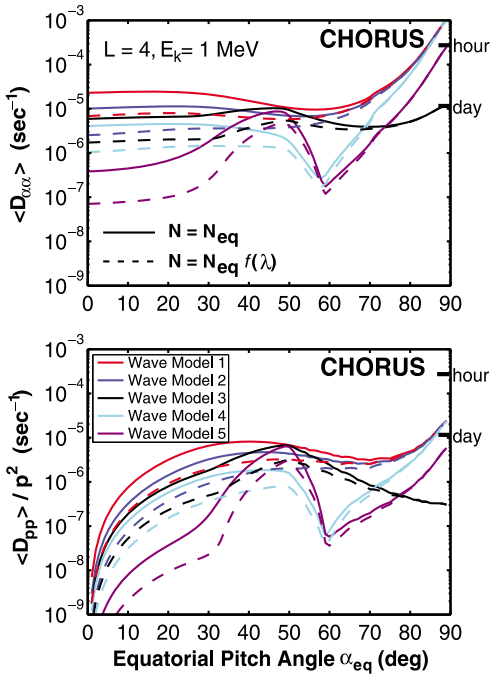

Fig. 4. Bounce-averaged pitch-angle diffusion rates (top) and momentum diffusion rates (bottom) for whistler-mode chorus for 1 MeV electrons at $L = 4$. The two chosen latitudinal distributions of particle density are as specified in Fig. 1, and the five wave models are as specified in Fig. 3.

$(1 + 3\sin^2\lambda)^{1/2}/\cos^6\lambda$ where λ is the magnetic latitude. We take $N_{eq} = 39\ \mathrm{cm}^{-3}$ and $\alpha^*_{eq} = (\Omega_e^2/\omega_{pe}^2)_{eq} = 0.058$ at $L = 4$. The effect of increasing particle density with latitude changes all three diffusion rates, the magnitude of the change depending on equatorial pitch-angle and electron kinetic energy. Larger changes occur at lower equatorial pitch-angles. This is because electrons with small values of α_{eq} bounce to higher latitudes where the density increases substantially in the case $N(\lambda) \propto f(\lambda)$. At all energies, an increase in particle density with latitude reduces the pitch-angle scattering rates near the loss cone but barely affects momentum diffusion rates for electrons with high equatorial pitch-angles ($70^\circ < \alpha_{eq} < 90^\circ$). Thus, an increasing latitudinal number density increases the loss timescales for electrons of all energies, but has little effect on acceleration of electrons mirroring at lower latitudes.

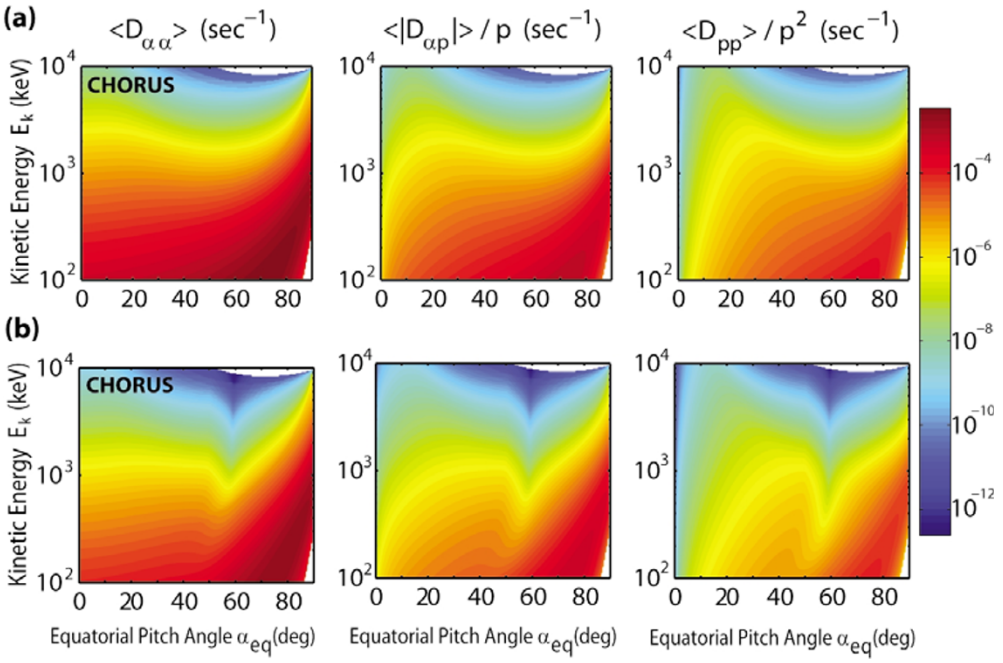

Fig. 5. Two-dimensional plots of bounce-averaged diffusion coefficients for whistler-mode chorus at $L = 4$ as functions of equatorial pitch-angle and kinetic energy. The assumed latitudinal density distribution is $N(\lambda) = N_{eq} f(\lambda)$ where $f(\lambda) = (1 + 3\sin^2\lambda)^{1/2}/\cos^6\lambda$. For the latitudinal distribution of chorus we adopt Wave Model 1 in the top panels and Wave Model 4 in the bottom panels (see Fig. 3).

In Fig. 2 for the same latitudinal distributions of particle number density used in Fig. 1 we calculate the pitch-angle and momentum diffusion rates for whistler-mode chorus for electron energies 200 keV, 1 MeV at a specified range of L-shells. We adopt the same chorus wave parameters used in Fig. 1 and we assume that the wave amplitude is constant along field lines. We use the equatorial "trough" particle density model $N_{eq} = 124(3/L)^4$ cm^{-3} due to Sheeley *et al.* (2001). Figure 2 shows generally that as L decreases, for both 200 keV and 1 MeV electrons, diffusion rates decrease. As an exception, for 1 MeV electrons momentum diffusion rates are largely independent of L-shell at large values of equatorial pitch-angle ($70^\circ < \alpha_{eq} < 90^\circ$), as was also found by Summers *et al.* (2007b).

In a study of the substorm dependence of chorus wave amplitudes Meredith *et al.* (2001) identifies equatorial ($|\lambda| < 15^\circ$) and high-latitude ($15^\circ < |\lambda| < 90^\circ$) chorus emissions outside the plasmasphere. We choose a set of five models of latitudinal distribution of wave amplitude to represent equatorial and high-latitude source strengths of chorus emissions of differing magnitudes. These models are illustrated in Fig. 3. For Model 1, $\Delta B(\lambda) =$ constant $=100$ pT. Models 2 and 3 respectively represent an equatorial source only and a high-latitude source only. Models 4 and 5 include both equatorial and high-latitude sources, but with different relative strengths. In Fig. 4 we plot bounce-averaged pitch-angle diffusion rates (top) and momentum diffusion rates (bottom) for whistler-mode chorus for 1 MeV electrons at $L = 4$. We adopt the same chorus wave parameters and latitudinal density distributions as used in Fig. 1, and we calculate the diffusion rates for each of the wave models given in Fig. 3. We see from Fig. 4 that the diffusion rates are influenced by the high-latitude wave distributions for small equatorial pitch-angles, and by the low-latitude wave distributions for large equatorial pitch-angles. For small (large) equatorial pitch-angles the diffusion rates increase as the overall strength of the high-latitude (low-latitude) wave distribution increases. In Fig. 4 the dependence of the diffusion rates on the latitudinal density distributions is similar to that found in Figs. 1 and 2.

In Fig. 5 we provide two-dimensional plots of the bounce-averaged diffusion coefficients for whistler-mode chorus at $L = 4$, versus equatorial pitch-angle α_{eq} and kinetic energy E_k. We assume the density distribution $N(\lambda) = N_{eq} f(\lambda)$, and for the waves we adopt Model 1 in the top panels and Model 4 in the bottom panels. Figure 5 shows how a change in the latitudinal wave distribution can produce significant changes in the diffusion coefficients over broad regions of (α_{eq}, E_k)-space.

3.2 Electron interaction with plasmaspheric hiss

Reinisch *et al.* (2001) and Denton *et al.* (2006) have carried out experimental studies of the plasma density distribution along field lines in the plasmasphere. Motivated by such studies, we adopt the functional forms $N(\lambda) = N_{eq}[f(\lambda)]^\sigma$ where $\sigma = 0, 0.6, 1, 1.5$, as representative of a realistic range of latitudinal density distributions in the plasmasphere at $L = 4$. We plot the electron number density profiles corresponding to these four models in Fig. 6. In the top and middle panels of Fig. 7 we present bounce-averaged pitch-angle diffusion rates for plasmaspheric hiss for electron energies 200 keV, 500 keV, and 1 MeV at $L = 4$. A Gaussian wave spectral density is assumed with $\omega_1/2\pi = 100$ Hz, $\omega_2/2\pi = 2000$ Hz, $\omega_m/2\pi = 550$ Hz, $\delta\omega/2\pi = 300$ Hz. We set $N_{eq} = 346$ cm^{-3} and $\alpha^*_{eq} = 0.0066$. In the top panel we put $\Delta B = 40$ pT, $|\lambda| < 15^\circ$; $\Delta B = 50$ pT, $15^\circ < |\lambda| < 90^\circ$ (Meredith *et al.*, 2004), and we use the four latitudinal density distributions shown in Fig. 6. In the middle panel we put $N(\lambda) = N_{eq} =$ con-

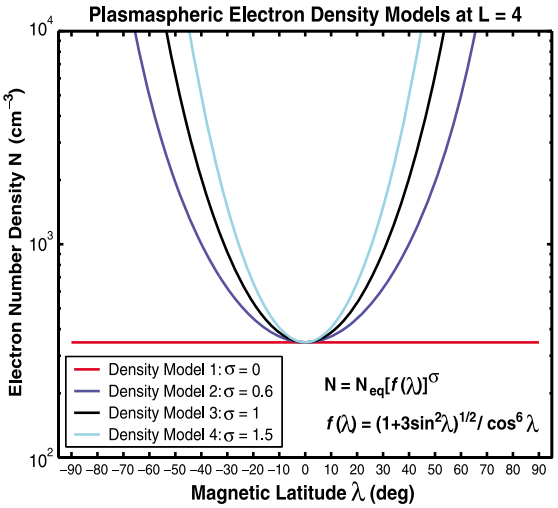

Fig. 6. Four models for the latitudinal distribution of plasmaspheric electron density at $L = 4$.

stant, and we specify four latitudinal distributions of hiss wave power. The wave models comprise Wave Model I: [$\Delta B = 10$ pT, $|\lambda| < 90°$]; Wave Model II: [$\Delta B = 40$ pT, $|\lambda| < 15°$; $\Delta B = 50$ pT, $15° < |\lambda| < 30°$; $\Delta B = 0$, $30° < |\lambda| < 90°$]; Wave Model III: [$\Delta B = 40$ pT, $|\lambda| < 15°$; $\Delta B = 50$ pT, $15° < |\lambda| < 90°$]; Wave Model IV: [$\Delta B = 100$ pT, $|\lambda| < 90°$]. Wave Models I–IV represent a range of hiss distributions from weak (I) to relatively strong (IV). No drift-averaging is carried out in Fig. 7. In the top panel of Fig. 7 we see that as the density distributions become stronger, diffusion rates become weaker at lower equatorial pitch-angles, for all energies, while at higher equatorial pitch-angles diffusion rates are largely independent of density distribution (as we found in Fig. 1 for chorus). Similarly, in the middle panel of Fig. 7, as the wave distributions become stronger the diffusion rates increase over a wide range of equatorial pitch-angles except those toward 90°. We note also in Fig. 7 (middle panel) that there is no distinction between the diffusion rates at energies 200 keV and 500 keV for the Wave Models II and III, whereas such a distinction exists at 1 MeV. The explanation is that MeV electrons are in resonance at higher latitudes ($|\lambda| > 30°$) whereas 200 keV, 500 keV electrons are not. Thus, the difference between Wave Models II and III is irrelevant for lower energy electrons.

In the bottom panel of Fig. 7 we show a two-dimensional plot of the bounce-averaged pitch-angle diffusion rate for hiss at $L = 4$, as a function of equatorial pitch-angle and kinetic energy. For this plot we adopt Wave Model III, which represents a fairly strong hiss distribution, and density model 2 with $\sigma = 0.6$ (see Fig. 6).

3.3 Electron interaction with EMIC waves

In the top and middle panels of Fig. 8 we present bounce-averaged pitch-angle diffusion rates for EMIC waves for electron energies 2.1 MeV, 3 MeV, 5 MeV, 10 MeV at $L = 4$. A Gaussian wave spectral density is assumed with $\omega_1 = \Omega_p/6$, $\omega_2 = \Omega_p/2$, $\omega_m = \Omega_p/3$, $\delta\omega = \Omega_p/6$ (where Ω_p is the proton gyrofrequency), and $\Delta B = 1$ nT. We set $N_{eq} = 346$ cm^{-3} and $\alpha^*_{eq} = 0.0066$. In the top panel

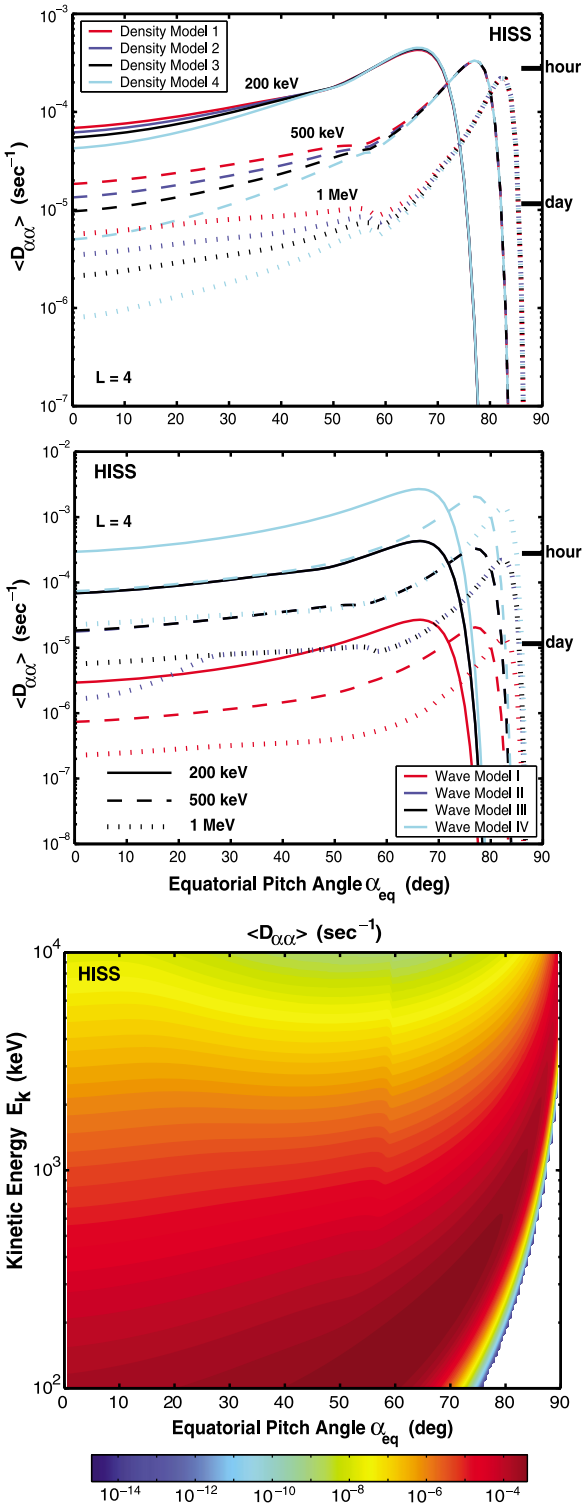

Fig. 7. In the top and middle panels, bounce-averaged pitch-angle diffusion rates for whistler-mode hiss for the indicated electron energies at $L = 4$. The plasmaspheric density models are as specified in Fig. 6. The four wave models are specified in the text. In the bottom panel, two-dimensional plot of the bounce-averaged pitch-angle diffusion rate for hiss at $L = 4$, corresponding to Wave Model III and Density Model 2.

we assume the wave amplitude is constant along the field line and we use the four latitudinal density distributions shown in Fig. 6. In the middle panel we put $N(\lambda) = N_{eq} =$ constant and we adopt the five latitudinal distributions of

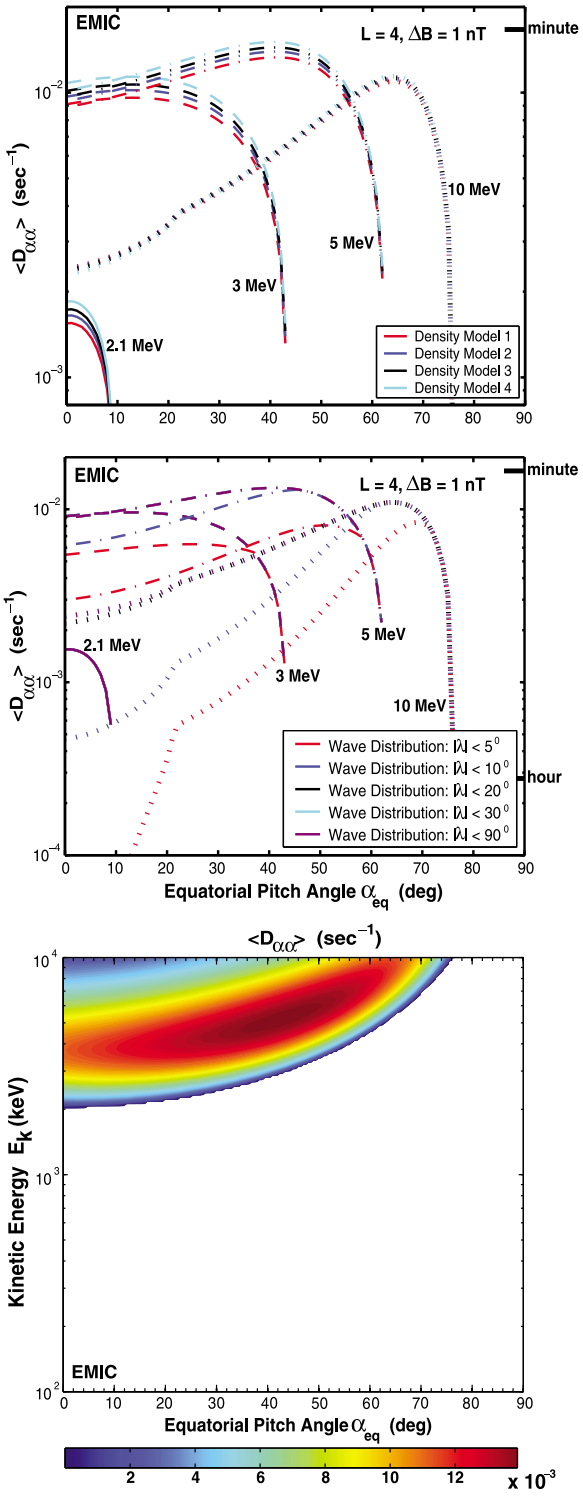

Fig. 8. In the top and middle panels, bounce-averaged pitch-angle diffusion rates for EMIC waves for the indicated electron energies at $L = 4$. The plasmaspheric density models are as specified in Fig. 6. In the bottom panel, two-dimensional plot of the bounce-averaged pitch-angle diffusion rate for EMIC waves at $L = 4$, corresponding to Wave Distribution $|\lambda| < 20^\circ$ and Density Model 2.

wave power indicated in the figure. No drift-averaging is carried out in Fig. 8. In Fig. 8 (top) for electron energies 2.1 MeV, 3 MeV, 5 MeV, diffusion rates increase as the density distribution becomes stronger (in contrast to the hiss diffusion rates in Fig. 7 (top)). At such energies EMIC wave-electron resonance occurs relatively close to the equator; a density increase then increases the region of resonance causing a corresponding increase in diffusion rate. However, for 10 MeV electrons, whose resonance region extends to higher latitudes, there is little distinction in the diffusion rate curves as the density distribution changes. For wave-particle interactions, in general, an increase in particle density causes a decrease in diffusion rate at any point. However, an increase in density may increase the latitudinal region of resonance and hence increase the diffusion rate. Whether or not a net increase in diffusion rate occurs depends partially on the competition between these processes. In Fig. 8 (middle), for 2.1 MeV electrons the diffusion rate curves are coincident for all five chosen wave distributions. This is because the region of resonance for 2.1 MeV electrons is approximately $|\lambda| < 5^\circ$. However, for 10 MeV electrons, whose resonance region extends to $|\lambda| \sim 30^\circ$, the diffusion rates increase substantially as the latitudinal range of the wave distribution increases. The differences and similarities between Fig. 7 and Fig. 8 regarding the influence on the diffusion rates of the density distributions and the wave distributions are largely controlled by the latitudinal regions of resonant electron-wave interaction.

In the bottom panel of Fig. 8 we show a two-dimensional plot of the bounce-averaged pitch-angle diffusion rate for EMIC waves at $L = 4$, for Wave Distribution $|\lambda| < 20^\circ$ and density model 2. The bottom panels of Fig. 7 and Fig. 8 provide a ready comparison between the scattering properties of hiss and EMIC waves for the adopted wave and density distributions.

In the present study we consider electron interaction with EMIC waves in a hydrogen plasma only. Electron scattering by EMIC waves can, in fact, be sensitively dependent on the ion composition of the plasma (Summers and Thorne, 2003; Summers *et al.*, 2007b). The influence of latitudinal distributions of particle density and wave power on electron scattering by EMIC waves in a multi-ion (H^+, He^+, O^+) plasma is left as an interesting topic for future study.

3.4 Electron loss timescales due to combined scattering by VLF chorus, ELF hiss and EMIC waves

We now consider electron precipitation loss timescales due to combined scattering by VLF chorus, ELF hiss and EMIC waves. In Fig. 9 (Case (I)) we show a schematic representation of the plasmasphere and typical distribution of waves for the case of low geomagnetic activity. Figure 9 (Case (II)) depicts the plasmasphere incorporating two drainage plumes, together with an expected distribution of waves. The plasmaspheric configurations in Fig. 9 were constructed from profiles presented by Spasojevic *et al.* (2003) that were deduced from IMAGE satellite data (see Summers *et al.* (2007b), section 5, for other examples of observed global configurations of the plasmasphere). The tables in Fig. 9 show the approximate percentage of an electron (circular) drift orbit that traverses each wave mode for $L = 3, 4, 5, 6, 7$. In Fig. 10 we present the total electron loss timescales, at energies 100 keV, 300 keV, 1 MeV, 3 MeV, due to combined scattering by the chorus, plasmaspheric hiss and EMIC wave distributions depicted in Cases (I) and (II) in Fig. 9. It is assumed that inside the plasmasphere (/plumes) the particle number density satisfies

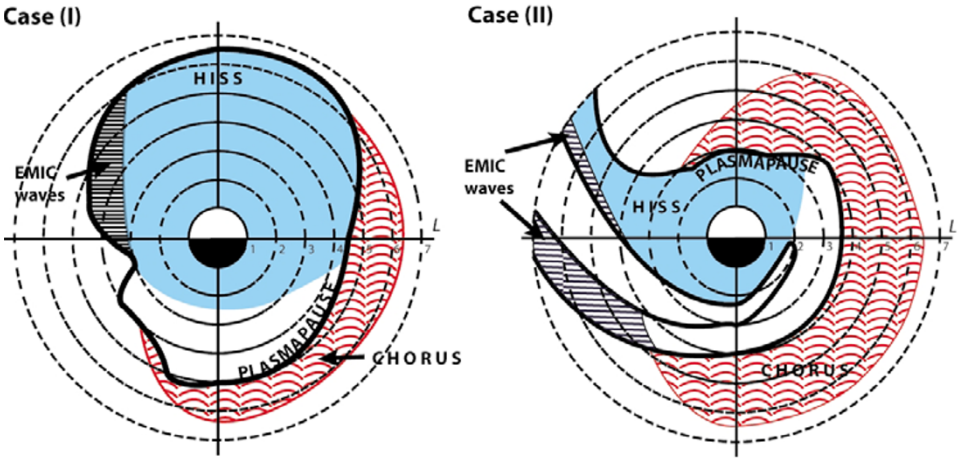

DRIFT-AVERAGE % FOR EACH WAVE MODE

	L = 3	4	5	6	7
chorus	0	0	32 %	39 %	0
hiss	66 %	45 %	32 %	23 %	0
EMIC waves	0	9 %	6 %	0	0

	L = 3	4	5	6	7
chorus	17 %	53 %	58 %	49 %	0
hiss	30 %	8 %	4 %	3 %	3 %
EMIC waves	0	1 %	10 %	8 %	5 %

Fig. 9. Schematic distributions of chorus, plasmaspheric hiss and EMIC waves in the case of low geomagnetic activity and expanded plasmasphere (Case (I)) and following high geomagnetic activity during the evolution of plasmaspheric plumes (Case (II)). For each case, the corresponding table shows the approximate percentage of an electron drift orbit that traverses each wave mode for a given L-value.

Table 1. The three wave models adopted in association with Figs. 9 and 10.

	Wave Model (a)	Wave Model (b)	Wave Model (c)
Chorus	$\Delta B(\lambda) = 100$ pT	Wave Model 4	Wave Model 5
Hiss	$\Delta B(\lambda) = 100$ pT	Wave Model III	$\Delta B(\lambda) = 10$ pT
EMIC	$\Delta B(\lambda) = 1$ nT	$\Delta B(\lambda) = 1$ nT	$\Delta B(\lambda) = 1$ nT

$N(\lambda) = N_{\rm eq}[f(\lambda)]^{\sigma}$, $N_{\rm eq} = 1390(3/L)^{4.83}$ cm^{-3}, and that outside the plasmasphere (/plumes) $N(\lambda) = N_{\rm eq}[f(\lambda)]^{\kappa}$, $N_{\rm eq} = 124(3/L)^4$ cm^{-3}. We adopt three sets of latitudinal distributions of wave power, namely, Wave Models (a), (b), (c) as specified in Table 1. We further assume that the chorus, hiss and EMIC waves have Gaussian spectral densities with the same parameters as used in the respective Figs. 1, 7, and 8. We calculate the total electron loss timescale $\tau_{\rm tot}$ using the method described by Summers *et al.* (2007b) (section 5). The method involves expressing the total electron scattering rate as the sum of the scattering rates due to each wave mode, each rate being evaluated at the equatorial loss cone angle. We estimate electron loss timescales by using the scattering rate at the edge of the loss cone only in those cases in which the pitch-angle diffusion rate is small over a high pitch-angle range narrower than $75^{\circ} < \alpha_{\rm eq} < 90^{\circ}$. Use of this criterion should ensure that electron lifetimes are controlled by scattering rates near the edge of the loss cone (e.g., Shprits *et al.*, 2006). In Fig. 10 the influence on the total electron loss timescale $\tau_{\rm tot}$ (which is inversely proportional to the total scattering rate) of the latitudinal distributions of density and wave power in general reflects the results obtained in Figs. 1, 2, 4, 7, and 8. For example, with some exceptions, the loss timescale increases as the latitudinal density distribution becomes stronger, or the latitudinal wave distribution becomes weaker, or the electron energy increases. A key factor controlling the results in Fig. 10 is that for a particular wave mode to contribute to the total scattering rate at a given L-value, an electron must not only traverse a region containing that wave mode, but the electron kinetic energy must exceed the minimum energy for resonance. In this regard, it is interesting to note the influence of EMIC waves in Case (I) and Case (II) in Fig. 10. In both Case (I) and Case (II) EMIC waves do not influence the loss timescales for 100 keV, 300 keV, and 1 MeV electrons since these energies are below the minimum resonant energy for electron-EMIC wave interaction. However, in Case (I) for $4 < L < 5$ and in Case (II) for $4 < L < 7$, EMIC waves resonantly scatter 3 MeV electrons with the result that since these waves are strong ($\Delta B = 1$ nT) the total electron loss timescale is significantly reduced. In Case (II) for 3 MeV electrons in the range $4 < L < 7$ since electron scattering is dominated by EMIC waves, and since also the region for EMIC wave-electron resonance is close to the equator, an increase in particle density at higher latitude has only marginal effect on the total loss timescale.

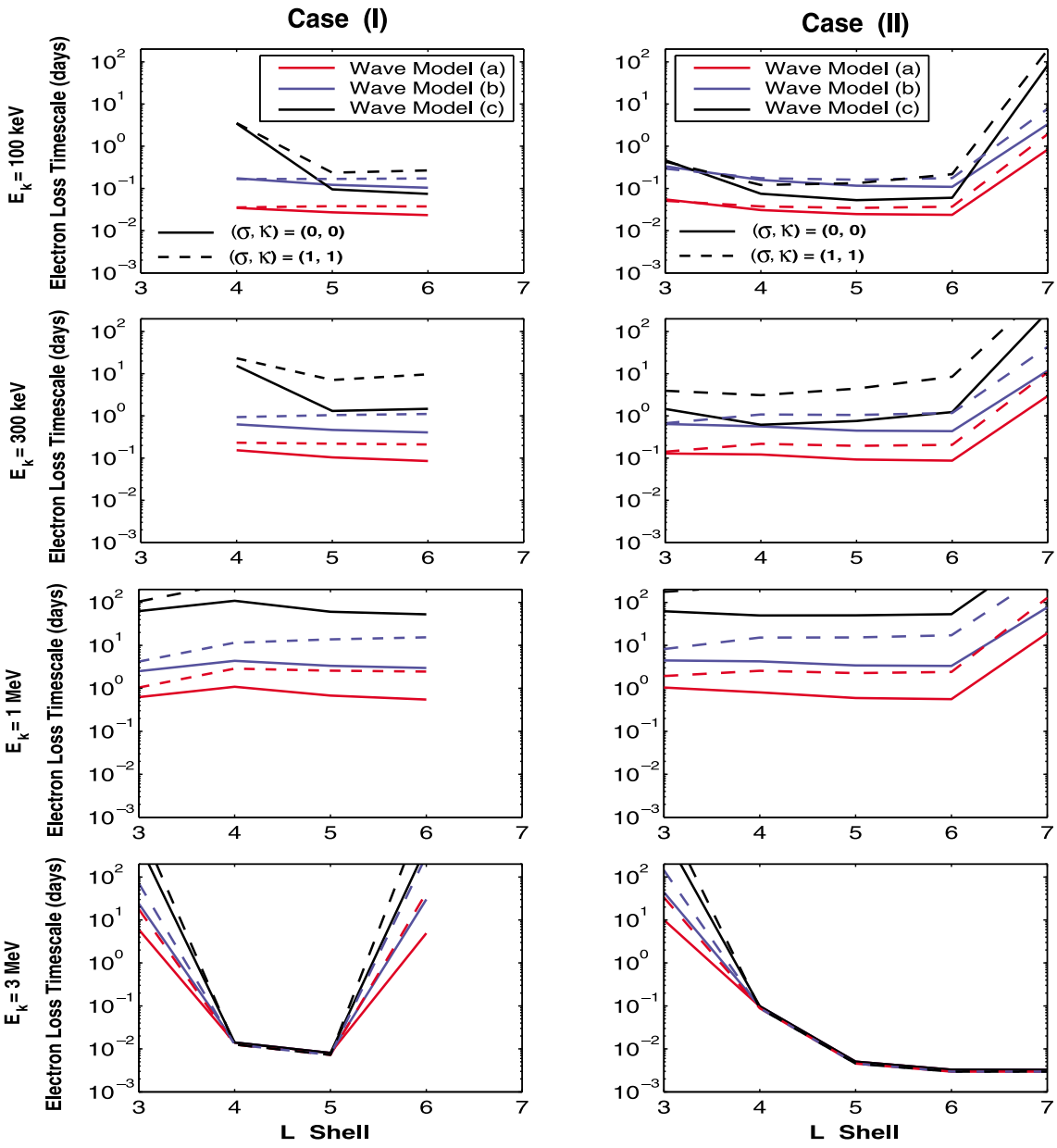

Fig. 10. Corresponding to Fig. 9, total electron loss timescales due to combined scattering by chorus, plasmaspheric hiss and EMIC waves in Case (I) and Case (II). The wave models (a), (b), (c) are given in Table 1 and the particle density models specified by σ and κ are described in the text.

4. Summary

We have examined the cyclotron resonant bounce-averaged diffusion rates of radiation belt electrons for VLF chorus, ELF hiss and EMIC waves, and we have adopted various latitudinal distributions of particle density and wave power. The diffusion rates can depend sensitively on the specified distributions of density and wave power. In general, however, the extent to which the distributions of density and wave power influence the diffusion rates depends on wave mode, equatorial pitch-angle, electron energy, and L-value. The bounce-averaged diffusion rates fundamentally depend on the spatial region over which cyclotron resonant wave-particle interaction can take place for any particular wave mode. The regions for resonance depend on wave band, electron energy, equatorial pitch-angle, and the local values of particle number density and magnetic field. Accurate determination of the cyclotron resonant diffusion rates of radiation belt electrons clearly requires detailed data on the global distribution of particle density and wave power. This study confirms the need for the acquisition of such data from future satellite missions.

Acknowledgments. This work is supported by the Natural Sciences and Engineering Research Council of Canada under grant A-0621.

References

Albert, J. M., Evaluation of quasi-linear diffusion coefficients for EMIC waves in a multispecies plasma, *J. Geophys. Res.*, **108**(A6), 1249, doi:10.1029/2002JA009792, 2003.

Albert, J. M., Simple approximations of quasi-linear diffusion coefficients, *J. Geophys. Res.*, **112**, A12202, doi:10.1029/2007JA012551, 2007.

Denton, R. E., *et al.*, Distribution of density along magnetospheric field lines, *J. Geophys. Res.*, **111**, A04213, doi:10.1029/2005JA011414, 2006.

Fraser, B. J. and T. S. Nguyen, Is the plasmapause a preferred source

region of electromagnetic ion cyclotron waves in the magnetosphere?, *J. Atmos. Sol. Terr. Phys.*, **63**, 1225–1247, 2001.

Horne, R. B., *et al.*, Timescale for radiation belt electron acceleration by whistler mode chorus waves, *J. Geophys. Res.*, **110**, A03225, doi:10.1029/2004JA010811, 2005.

Lyons, L. R., Pitch angle and energy diffusion coefficients from resonant interactions with ion-cyclotron and whistler waves, *J. Plasma Phys.*, **12**, 417–432, 1974.

Meredith, N. P., R. B. Horne, and R. R. Anderson, Substorm dependence of chorus amplitudes: Implications for the acceleration of electrons to relativistic energies, *J. Geophys. Res.*, **106**, 13165–13178, 2001.

Meredith, N. P., R. B. Horne, R. M. Thorne, D. Summers, and R. R. Anderson, Substorm dependence of plasmaspheric hiss, *J. Geophys. Res.*, **109**, A06209, doi:10.1029/2004JA010387, 2004.

Miyoshi, Y., *et al.*, Rebuilding process of the outer radiation belt during the 3 November 1993 magnetic storm: NOAA and Exos-D observations, *J. Geophys. Res.*, **108**(A1), 1004, doi:10.1029/2001JA007542, 2003.

Omura, Y. and D. Summers, Dynamics of high-energy electrons interacting with whistler mode chorus emissions in the magnetosphere, *J. Geophys. Res.*, **111**, A09222, doi:10.1029/2006JA011600, 2006.

Reinisch, B. W., *et al.*, Plasma density distribution along the magnetospheric field: RPI observations from IMAGE, *Geophys. Res. Lett.*, **28**(24), 4521–4524, 2001.

Roth, I., M. Temerin, and M. K. Hudson, Resonant enhancement of relativistic electron fluxes during geomagnetically active periods, *Ann. Geophys.*, **17**, 631–638, 1999.

Santolik, O., D. A. Gurnett, J. S. Pickett, M. Parrot, and N. Cornilleau-Wehrlin, A microscopic and nanoscopic view of storm-time chorus on 31 March 2001, *Geophys. Res. Lett.*, **31**, L02801, doi:10.1029/2003GL018757, 2004.

Sheeley, B. W., M. B. Moldwin, H. K. Rassoul, and R. R. Anderson, An empirical plasmasphere and trough density model: CRRES observations, *J. Geophys. Res.*, **106**, 25631–25642, 2001.

Shprits, Y. Y., W. Li, and R. M. Thorne, Controlling effect of the pitch angle scattering rates near the edge of the loss cone on electron lifetimes, *J. Geophys. Res.*, **111**, A12206, doi:10.1029/2006JA011758, 2006.

Spasojevic, M., *et al.*, Global response of the plasmasphere to a geomagnetic disturbance, *J. Geophys. Res.*, **108**(A9), 1340, doi:10.1029/2003JA009987, 2003.

Summers, D., Quasi-linear diffusion coefficients for field-aligned electromagnetic waves with applications to the magnetosphere, *J. Geophys. Res.*, **110**, A08213, doi:10.1029/2005JA011159, 2005.

Summers, D. and C. Ma, A model for generating relativistic electrons in the Earth's inner magnetosphere based on gyroresonant wave-particle interactions, *J. Geophys. Res.*, **105**, 2625–2640, 2000.

Summers, D. and R. M. Thorne, Relativistic electron pitch angle scattering by electromagnetic ion cyclotron waves during geomagnetic storms, *J. Geophys. Res.*, **108**(A4), 1143, doi:10.1029/2002JA009489, 2003.

Summers, D., R. M. Thorne, and F. Xiao, Relativistic theory of wave-particle resonant diffusion with application to electron acceleration in the magnetosphere, *J. Geophys. Res.*, **103**, 20487–20500, 1998.

Summers, D., *et al.*, Model of the energization of outer-zone electrons by whistler-mode chorus during the October 9, 1990 geomagnetic storm, *Geophys. Res. Lett.*, **29**(24), 2174, doi:10.1029/2002GL016039, 2002.

Summers, D., B. Ni, and N. P. Meredith, Timescales for radiation belt electron acceleration and loss due to resonant wave-particle interactions: 1. Theory, *J. Geophys. Res.*, **112**, A04206, doi:10.1029/2006JA011801, 2007a.

Summers, D., B. Ni, and N. P. Meredith, Timescales for radiation belt electron acceleration and loss due to resonant wave-particle interactions: 2. Evaluation for VLF chorus, ELF hiss, and electromagnetic ion cyclotron waves, *J. Geophys. Res.*, **112**, A04207, doi:10.1029/2006JA011993, 2007b.

Thorne, R. M., T. P. O'Brien, Y. Y. Shprits, D. Summers, and R. B. Horne, Timescale for MeV electron microburst loss during geomagnetic storms, *J. Geophys. Res.*, **110**, A09202, doi:10.1029/2004JA010882, 2005.

D. Summers (e-mail: dsummers@math.mun.ca) and B. Ni